# Trifluoroethanol-Induced Unfolding of Concanavalin A: Equilibrium and Time-Resolved Optical Spectroscopic Studies†

Qi Xu and Timothy A. Keiderling*

*Department of Chemistry, University of Illinois at Chicago, 845 West Taylor Street (m/c 111), Chicago, Illinois 60607-7061*

*Received January 3, 2005; Revised Manuscript Received March 18, 2005*

ABSTRACT: Conformational structure changes in concanavalin A (Con A), a legume lectin protein which is composed of 18 $\beta$-strands, induced by dissolving in 50% trifluoroethanol (TFE) were monitored at neutral and low pH by far- and near-UV circular dichroism (CD), fluorescence, and FTIR under equilibrium conditions. Stopped-flow studies using CD and fluorescence as well as FTIR, at low and high protein concentration, respectively, were carried out to follow the time-dependent conformation changes occurring after rapid mixing of the protein with TFE. Equilibrium CD results show that, upon addition of TFE, low-concentration Con A transforms to a highly $\alpha$-helical conformation at both neutral and low pH. However, at neutral pH under high protein concentration conditions, aggregation and precipitation are eventually detected with FTIR, indicating that a final $\beta$-structure is attained. Stopped-flow fluorescence shows the existence of an unfolding intermediate for pH 2.0 and 4.5, which could be related to the dissociation of the dimer form. However, evidence for an intermediate is not obtained at pH 6.7, where the native protein is a tetramer. Stopped-flow FTIR is consistent with these results, indicating formation of a $H^+$-stabilized intermediate $\alpha$-helical conformation before aggregation develops. Con A in TFE provides an example of an intermediate with non-native secondary structure appearing on the unfolding pathway. On the basis of the kinetic results obtained, an unfolding mechanism is proposed and some stable intermediates are identified. In turn, the slow structural change of Con A induced by TFE provides a useful model system for study of protein unfolding due to its accessibility with several spectroscopic and kinetic tools.

Cosolvents, especially 2,2,2-trifluoroethanol (TFE[1]), have been used in several attempts to characterize secondary structure in protein folding transition states (*1*−*12*). TFE is known to stabilize $\alpha$-helical structure in proteins and their fragments, but this effect can be specific, not fully general. For example, fragments arising from the helical region of the native structure of lysozyme have a high tendency to form a helix in the presence of TFE, while those from the $\beta$-region have a low tendency (*13*). These results suggest that nativelike secondary structure can be formed in some regions of the unfolded protein and serve as initiation sites for protein folding (*14*). Shiraki and Goto (*4*) measured the TFE-induced conformational transition of over 20 proteins of various secondary structural types, and found that the helical content in TFE was correlated more with the helical content predicted by a secondary structure prediction algorithm than with the helical content of the native structure, which suggests that the stability of helical structure formed in TFE is determined by local rather than extended or tertiary-structure-facilitated interactions. Although TFE-induced stabilization of helical structure is known for some $\beta$-sheet proteins, especially for $\beta$-lactoglobulin (*4*, *15*), little comprehensive work has been carried out for study of solvent effects on proteins composed predominantly of $\beta$-sheet structure.

Legume lectins, a class of oligomeric proteins that bind carbohydrates specifically and reversibly, have been implicated in various biological recognition processes (*16*). Concanavalin A (Con A), the lectin from *Canavalia ensiformis* (jack bean), is the best studied member of this group. Con A contains manganese and calcium near the carbohydrate binding site, and its three-dimensional structure has been determined by X-ray diffraction analysis at 1.2 resolution for crystals held under 120K (*17*). The monomer has a jelly roll motif composed of three antiparallel $\beta$-sheets, including a six-stranded flat "back" and a seven-stranded curved "front" $\beta$-sheet with a five-stranded $\beta$-sheet "roofing" the other two (Figure 1a). In acidic conditions, pH < 6, Con A exists in a dimer form (Figure 1b), characterized by a large 12-stranded $\beta$-sheet resulting from the antiparallel edge-to-edge alignment of the two flat six-stranded $\beta$-sheets, one from each monomer. At physiological pH, Con A exists as a tetramer (Figure 1c), formed by two canonical dimers joining the central parts of their back sheets in a perpendicular manner (*18*). Under basic conditions, pH between 8 and 9, an apparent irreversible conformational transition occurs, which results in aggregation and precipitation (*19*).

Although extensive studies of interactions between Con A and carbohydrate molecules have been reported, little is

† This research was supported in part by grants from the Research Corporation and the National Science Foundation (CHE00-91994) for instrument purchases, and the Guggenheim Foundation for a fellowship to T.A.K. aiding manuscript preparation.

* To whom correspondence should be addressed. Phone: (312) 996-3156. Fax: (312) 996-0431. E-mail: tak@uic.edu.

[1] Abbreviations: CD, circular dichroism; Con A, concanavalin A; FTIR, Fourier transform infrared; TFE, trifluoroethanol.

10.1021/bi050003u CCC: $30.25 
Published on Web 05/13/2005

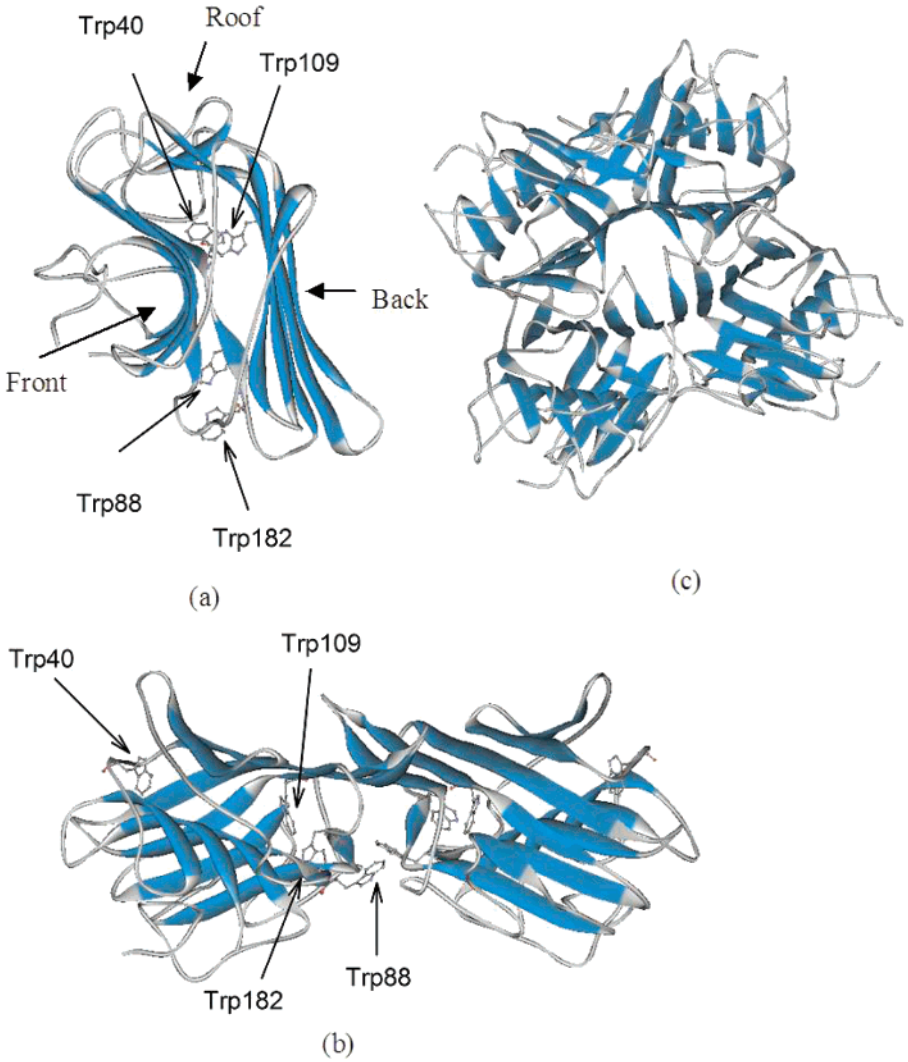


FIGURE 1: (a) Tertiary structure of monomer concanavalin A, which consists of a flat six-stranded "back" $\beta$-sheet, a curved seven-stranded "front" $\beta$-sheet, and a five-stranded "top" $\beta$-sheet. (b) Dimer conformation of Con A, which involves edge-to-edge alignment of the flat six-stranded back $\beta$-sheets forming a contiguous 12-stranded sheet. The Trp residues are indicated by the framework side chains and labeled in one monomer. (c) The tetramer of Con A consists of back-to-back association of two dimers. The structures shown are from the Protein Data Bank, 1APN (dimer) and 1AZD (tetramer).

known about the protein stability and its folding/unfolding. A $\beta$-sheet to $\alpha$-helical transition for Con A at low pH mixed into a TFE-containing solution was observed by circular dichroism (CD) (*4*) and FTIR (*20*) under equilibrium conditions. However, no comprehensive work, especially no dynamic studies, has been carried out to describe such changes. In this paper, we systematically investigate, by use of equilibrium and time-resolved circular dichroism, fluorescence, and FTIR techniques, the conformational changes of Con A induced by addition of TFE. These sample the structure on different levels, fluorescence and near-UV−CD sensing tertiary structure and far-UV−CD and FTIR sensing secondary structure, with different physical mechanisms. Their contribution can offer new insight into this perturbed folding problem.

In addition to the observation of a $\beta$-sheet to $\alpha$-helix transition, which has been previously reported (*2*, *11*, *12*), a slow process resulting in an $\alpha$-helix changing to an aggregation state is recorded here. The latter is additionally shown to be dependent on both the pH and protein concentration. This finding is important because this aggregation formation mechanism might be related to amyloid formation as suggested by more recent reports for other protein systems (*6*, *8*, *21*). Meanwhile, for the first time to our knowledge, this work presents a $\beta$-sheet to $\alpha$-helix transition studied by stopped-flow FTIR analysis of the whole amide I band, where helical and sheet contributions can be resolved and their kinetics correlated to CD and fluorescence changes.

From these data, we propose that the TFE-induced $\alpha$-helical form behaves as a stable unfolding intermediate. This process of sheet to helix to aggregate does not fit the usual hierarchical model but may be useful for development of the growing appreciation of aggregation mechanisms now appearing (*21*−*25*). Finally, the effect of TFE on the protein structure is discussed, providing a summary of previous models and their reflection on our data, but the general TFE mechanism remains unclear.

## MATERIAL AND METHODS

*Materials.* Concanavalin A (jack bean) and trifluoroethanol were purchased from Sigma and used without further purification. $D_2O$ and DCl were purchased from Cambridge

Isotope Laboratories, Inc. TFE-OD was obtained by distilling TFE with $D_2O$, and collecting the elutant at 78−79 °C. All the pH values in this paper represent apparent pH meter readings, no correction was made for solutions prepared in $D_2O$, and all readings for mixed solutions represent the value before addition of TFE. Due to the relative stability of Con A with pH, vide infra, any variations at either the neutral (pH ≈ 7) or low (pH ≈ 2) regimes are of little consequence and, with 50% TFE, of little meaning. In aqueous solution, to obtain different pH conditions, Con A was dissolved in 10−20 mM phosphate buffer (pH ≈ 7), acetic buffer (pH 3−4), or 10−20 mM HCl (pH ≈ 2). For Con A in TFE, the pH value used to characterize the solution was that of the Con A solution before addition of TFE and was not remeasured after mixing. For IR measurements, Con A was dissolved in $D_2O$ for half an hour before the addition of TFE to deuterate all readily exchangeable sites. Although complete H/D exchange is not obtained, especially for sites buried due to protein dimer and tetramer formation at low temperatures, our studies (unpublished data) indicate that there is no noticeable amide I′ peak shift for Con A (which is primarily $\beta$-sheet) in going from $H_2O$ and $D_2O$, in contrast to the normal ∼5 $cm^{-1}$ shift in helical proteins. All the measurements were carried out at room temperature unless otherwise mentioned. Samples mixed with TFE were measured shortly after preparation, so that rapid kinetic changes were complete, but long-term aggregation processes could be ongoing. In any cases where such changes were seen, the results are specifically noted; otherwise the spectra were stable for the duration of the experiments.

*Fluorescence Measurements.* Fluorescence measurements were performed on a Fluoromax-2 spectrofluorimeter (Jobin Yvon, New Jersey). Samples with and in the absence of TFE were placed in a 4 mm path length cylindrical cuvette, and emission spectra over the range of 300−450 nm were recorded using excitation at 290 nm, with excitation and emission resolutions (slit width) of 5 nm. The fluorescence spectra shown are an average of three scans after subtraction of the corresponding blanks.

*CD Measurements.* CD experiments were performed on a J-810 spectropolarimeter (Jasco, Maryland). Protein concentrations of 0.2 and 2 mg/mL, with a path length of 1 mm and 1 cm, were used for CD measurement in the far- and near-UV regions, respectively. Averages of 4 or 12 scans were used for far-UV CD or near-UV CD measurements, the final results being obtained by subtraction of identically obtained scans of blanks from the spectra.

*Stopped-Flow CD and Fluorescence.* An SFM-400 stopped-flow mixer (Bio-logic, France) with an SF-20 fluorescence cell was attached to the J-810 CD spectropolarimeter and used for the stopped-flow CD and fluorescence experiments under control of Jasco kinetics software. The whole stopped-flow system was thermostated by means of a temperature-controlled water bath and high-flow circulating pump (Neslab, RT-111) to control the temperature of the cell and syringes. A 150 W Xe−Hg lamp was used to obtain more excitation intensity at ∼225 nm and improve the signal to noise ratio (S/N). The dynamic CD signal was recorded at 222 nm, and the total fluorescence signal was collected at 90° to the excitation by use of a cutoff filter (>320 nm). The time-dependent results were fit with multiple exponential functions using the Bio-Kin32 software (Bio-logic, France).

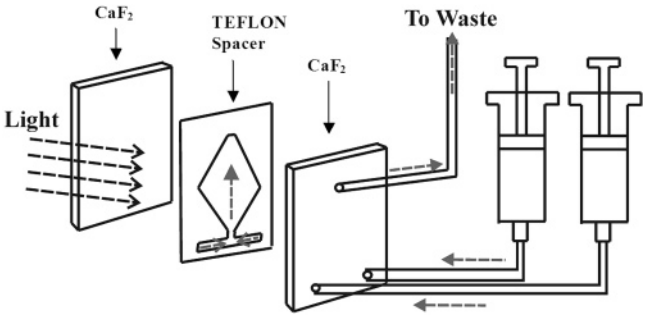


FIGURE 2: Design schematic of the stopped-flow mixer for FTIR. The top $CaF_2$ (15 × 25 mm) window was drilled with two holes on the bottom and one hole on the top. Protein solution and TFE were injected into the IR cell separately through the two bottom holes by use of two 250 $\mu$L SGE syringes mounted externally and connected to the metal compression/cover plate (not shown) by Teflon FEP tubing (1.6 mm o.d., 0.5 mm i.d.). A 140 $\mu$m Teflon spacer sandwiched between the top and back $CaF_2$ plates was used to lead the solutions to a "T" mixer before the mixture filled the detection window which is defined by both the diamond-shaped spacer and a rectangular opening (9 × 13 mm) on the metal compression plate (not shown). The waste solution leaves the cell through the top hole. The arrows shown in the figure indicate the direction of solution flow.

*Fourier Transform Infrared Absorption*. For FTIR spectra, Con A was dissolved directly into $D_2O$ to a final protein concentration of 10 mg/mL with, or in the absence of, 50% TFE and placed in a sealed cell composed of two $CaF_2$ windows and a Teflon spacer. DCl was used to adjust the pH to acidic values (pH ≈ 2), and 10−20 mM phosphate and acetic buffer solution were used for neutral pH and pH ≈ 4 solution, respectively. The IR absorption spectra were recorded at 4 $cm^{-1}$ nominal resolution as an average of 512 scans using a Digilab (Randolph, MA) FTS-60A FTIR spectrometer with a DTGS detector. A path length (spacer) of 50 $\mu$m was used, except for measurements of the effects of pH and Con A concentration, where a 100 $\mu$m path length was used and where all spectra were recorded at the same time after mixing of Con A with TFE. For temperature variation studies, the cells were tightly fit into a homemade double-walled brass jacket through which water was pumped from a thermostatically controlled Neslab RTE-7 water bath. Programmed heating was used to change the temperature of the cell, and a thermocouple placed in the outer jacket of the cell was used to control the bath to achieve a constant sample temperature.

*Stopped-Flow FTIR*. All kinetic IR experiments were performed using the Digilab FTS 60A spectrometer and WinIR Pro kinetic software, with an external beam coupled to a homemade sample compartment containing sharply focused optics (parabolic mirrors) and a sensitive, 1 $mm^2$ liquid nitrogen cooled MCT detector. A homemade flow-through IR cell was used, with a T-shaped mixer built into part of the spacer, as shown in Figure 2. Small aperture $CaF_2$ windows were used with a spacer of 140 $\mu$m, resulting in a sample volume of ∼11 $\mu$L, with a <20 ms mixing dead time. However, due to window fluctuation caused by high-speed solution injection, stable FTIR spectra could only be obtained 100 ms after mixing. With the optimal instrument parameters (resolution 8 $cm^{-1}$, scan speed 125 kHz, single-sided acquisition mode), each spectrum could be obtained within 50 ms in kinetic scan mode, which for continuous scan operation also becomes the interval between successive scans.

In the stopped-flow experiments, $D_2O$ and TFE-OD were first mixed at a 1:1 ratio to obtain a background spectrum, and then the IR cell was flushed with $D_2O$ to get rid of the residual TFE-OD. Finally 50 $\mu$L of 10 mg/mL Con A solution in $D_2O$ was mixed with 50 $\mu$L of TFE-OD, and the IR spectra were recorded every 50 ms to monitor the fast change with a total collection time of up to ~10 s. The instrument started collecting spectra before the mixing syringes were driven manually. For timing, the last point before the intensity jump was set to be $t = 0$ for the mixing. Spectra were subsequently truncated to 1600−1700 $cm^{-1}$ and stored, all under control of the Digilab kinetic software. For monitoring the slow changes, the spectra were recorded more conventionally after recording of the fast change, commencing 1 min after the mixing, and collected every 5 s at 40 kHz scan speed.

Separation of spectral components was done using principle component or factor analysis (*26*). By diagonalization of the covariance matrix of all the spectra in the data set, each spectrum can be decomposed into a linear combination of components, ranked in decreasing order of significance (*27*, *28*). The first component represents the average spectral intensity, and the second is the major variance to that. Its loading correlates to the time-dependent variation in the entire spectral shape, corresponding to the major kinetic process, as sensed by the IR. If a segment of the amide I spectrum is selected, the spectral variation weighted for helical and sheet contributions can be separately analyzed. Kinetic analysis of the change in loading of the second component with time was done with the SIGMAPLOT software. Due to the large number of spectra obtained and fast change observed, only every other point for the first ~5 s was used in the fit (out of a total of ~200 spectra for ~10 s of measurement).

*Two-State Transition Analysis*. The change in the experimental signal ($I_b$), representing the intensity of the aggregation peak in the IR spectra, as a function of temperature, was fit to a two-state unfolding equilibrium model with six variable parameters, assuming a $\Delta C_p = 0$, according to

$$I_b = \frac{(m_a T + C_a) + (m_b T + C_b)\exp\left[\frac{\Delta H_m^\circ}{R}\left(\frac{1}{T_m} - \frac{1}{T}\right)\right]}{1 + \exp\left[\frac{\Delta H_m^\circ}{R}\left(\frac{1}{T_m} - \frac{1}{T}\right)\right]}$$

where $\Delta H_m^\circ$ is the enthalpy at the transition midpoint, $T_m$. The remaining four parameters, $m_a$, $C_a$, $m_b$, and $C_b$, represent the baseline parameters (slope and offset) for the assumed-linear, temperature-dependent changes of the initial (here intermediate) state a (α-helix form) and final state b (partial aggregation). The aggregation peak is assigned to the sharp amide I′ feature that grows in at ~1615 $cm^{-1}$.

## RESULTS

Parts a and b (inset) of Figure 3 show the far- and near-UV−CD spectra of Con A, with and in the absence of 50% TFE added to the protein solution at both pH 6.5 (tetramer) and pH 2 (dimer). When no alcohol is present, Con A shows identical far-UV CD spectra at both pHs with its well-known atypical $\beta$-sheet band shape (having a negative extremum at 223 nm and a positive peak at 200 nm). The overlapped CD

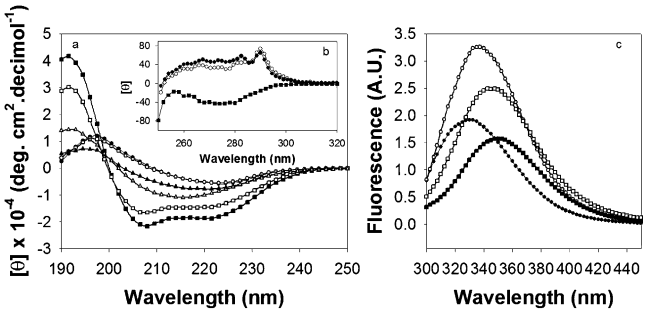


FIGURE 3: (a) Far-UV CD, (b) (inset) near-UV CD, and (c) fluorescence spectra of (0.2 mg/mL) Con A, at pH 6.5 (open symbols) and pH 2 (filled symbols), in the absence of (circles) and with 10% (triangles) and 50% (squares) added TFE (see the Materials and Methods for sampling details).

spectra (circles) indicate that an acidic pH change has no influence on Con A secondary structure, which is consistent with the previous reports (*29*) and our own titration results (not shown). Addition of 10% TFE first transforms the CD spectra to a shape more typical of a $\beta$-sheet conformation with a negative peak at 215 nm for both pHs. (Methanol has a similar effect, which we have studied separately (*30*).) A transition to typical α-helical spectra was obtained at 15% and 30% TFE for acidic and neutral pHs, respectively. After that, a gradual increase of α-helix content with the addition of more TFE was observed and the spectral amplitude became stabilized at ~40% and 50% TFE for pH 2 and 6.5, respectively (data not shown). In 50% TFE (squares), the CD spectra are characteristic of a highly α-helical structure at both neutral and low pH, and differ sharply from the $\beta$-like CD spectrum seen for Con A in water. Since 50% is seemingly a point of complete conversion from a native sheet fold to a predominantly helical one for Con A, it is the TFE concentration used in the subsequent mixing experiments discussed below, although changes at intermediate concentrations certainly could be of interest.

Although spectra characteristic of α-helical conformation were recorded for Con A in 50% TFE at pH 6.5, the intensity of the α-helical component decreased with time, and the protein precipitated after several hours with stirring, suggesting there is a slow α → aggregation transition. Evaluation of the CD results with the Selcon3 program (*31*) suggested a more highly helical content for Con A at low pH (filled symbols) than at neutral pH (open symbols) in 50% TFE, the fit yielding 57% vs 43%, respectively, implying that the helicity in Con A is enhanced when the polypeptide is protonated.

The tertiary structure change, as monitored by the near-UV−CD change of Con A with and in the absence of 50% TFE, is shown in Figure 3b. In the absence of TFE (circles), positive maxima at 289 and 282 nm were observed, as well as a broad band from 280 to 260 nm, indicating that aromatic residues are in a specific packing arrangement symptomatic of the tertiary structure. Only a small change is observed on reducing the pH, indicating only a minor effect on the aromatic groups, which report on the tertiary structure. However, when 50% TFE is added (solid squares) at pH 2, a broad negative band from 295 to 260 nm is observed, suggesting a significant tertiary structure change, which is consistent with and would facilitate the secondary structure change detected in the far-UV region. For this near-UV−

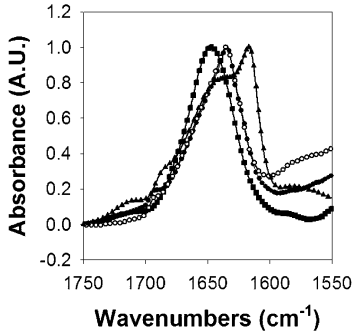


FIGURE 4: Amide I′ FTIR absorbance spectra of 10 mg/mL Con A in the absence of (circles) and with (squares) 50% TFE, at pH 7 (open symbols) and pH 2 (filled symbols), and at pH 3.7 in 50% TFE (triangles). Each band was normalized to a maximum of 1.0 for comparison (see the Materials and Methods for sampling details).

CD experiment, precipitation is obtained when TFE is added to Con A at neutral pH, due to the much higher protein concentration used to obtain measurable spectra, a condition discussed later.

The four Trp residues per subunit of Con A which give rise to the near-UV−CD also fluoresce, providing an additional sensitive monitor of tertiary structure change. The fluorescence spectra of Con A with and in the absence of 50% TFE at both neutral and low pH are shown in Figure 3c. Although far- and near-UV−CD spectra do not change very much with pH, the fluorescence spectra do have larger variations. About 40% intensity loss as well as a blue shift (from 337 to 331 nm) occurs when pH is changed from 6.5 to 2.0, which is correlated to the small change detected by near-UV−CD. Since there is no secondary structure change, this is probably due only to solvation (protonation) effects on the Trp fluorophores. When 50% TFE is added, a large red peak shift as well as an intensity loss is observed for both pH values, indicating that a more polar environment is attained for Trp residues in TFE than the native condition (*32*, *33*). This is consistent with opening of the tertiary structure in the TFE environment, thereby solvating the aromatic side chains, much as in the condition often assumed when formation of a molten globule state is assigned (*34*, *35*).

Figure 4 shows the FTIR spectra of Con A at apparent pH 7 and 2 with and in the absence of 50% TFE-OD, and additionally for Con A at pH 3.7 with 50% TFE (triangles). Identical amide I′ (N-deuterated) bands are observed for Con A at 1634 $cm^{-1}$ for both neutral and low pH (circles), indicating a dominant $\beta$-sheet structure independent of pH, consistent with what is seen with CD and with previous reports (*29*). In 50% TFE at pH 2, an amide I′ peak is observed at 1649 $cm^{-1}$ (squares), indicating conversion to a partial α-helical conformation, paralleling the CD interpretation and confirming the same process occurs in both concentration regimes. In 50% TFE at pH > 4, Con A precipitated, as noted in the near-UV−CD results above, but with the apparent rate of aggregation accelerated by the higher concentration needed for the FTIR experiments. For pH values between 3 and 4, precipitation was not observed, but a sharp aggregation-related peak at 1617 $cm^{-1}$ and a shoulder at 1688 $cm^{-1}$ (*36*, *37*) were evident in the spectrum (illustrated in Figure 4, triangles). In the lower concentration

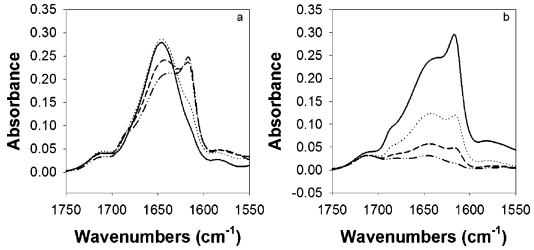


FIGURE 5: (a) FTIR amide I′ spectra of 10 mg/mL Con A in 50% TFE-OD at pH 3.6 (dashed−dotted−dashed line), 3.3 (dashed line), 3.0 (dotted line), and 2.8 (solid line). (b) FTIR spectra of 10, 5, 2.5, and 1.25 mg/mL Con A (from top to bottom) in 50% TFE-OD at pH 3.6. All the spectra were obtained at the same time after mixing of the TFE with protein. The pH of the solution is the apparent reading on the pH meter before mixing of the protein 1:1 with TFE.

CD conditions, the pH 3−4 results reflect those obtained at low pH.

The protein conformations obtained in differing solvents as would be derived from the above CD and FTIR results have some variances which can be explained by the difference in sample conditions used in the two methods. The effects of pH and protein concentration on the conformation of Con A unfolded by TFE (50%) were studied with FTIR as shown in parts a and b, respectively, of Figure 5. At [ConA] = 10 mg/mL (Figure 5a), lowering the pH increased the helical amide I′ peak and removed the aggregation peak, indicating that low pH hinders aggregation. Tests with various protein concentrations but fixed pH 3.6 are shown in Figure 5b, where the aggregation peak is observed to disappear at lower protein concentration, suggesting that high protein concentration favors aggregation, as would be expected.

*Thermal Denaturation*. Thermal variation of Con A in 50% TFE was monitored by both CD and FTIR, for low and high concentration conditions, respectively. The changes in ellipticity at 222 nm with an increase of temperature for Con A in 50% TFE at both low (filled circles) and neutral (open circles) pH are plotted in Figure 6a. At low temperature, the far-UV−CD spectra show characteristic α-helical spectra, and an overall loss of ellipticity was observed with an increase of temperature. An isodichroic point was observed at ∼202 nm, suggesting a possible two-state transition. However, even at 80 °C, remnants of the α-helical-type spectral band shape remained, with relatively more loss (than indicated in Figure 6a) for the positive band at 190 nm, implying formation of a coil-like final state. No visible precipitation was observed. On cooling back to 5 °C, most of the intensity was recovered at both pHs.

For higher Con A concentration in 50% TFE at pH 1.8, the FTIR intensity of the amide I′ band decreases with an increase of temperature and the spectrum broadens, both of which are consistent with inducing disorder, partially unfolding the helix form, as shown in Figure 6b, but there is little peak frequency shift and no aggregation peak was observed even up to 80 °C. However, when cooled back to 20 °C, the low-temperature FTIR spectrum was not fully recovered, due to the residual, helical amide I′ band shifting ∼5 $cm^{-1}$ to lower frequency, suggesting further H/D exchange occurred after unfolding (due at high temperature to exposure to solvent of initially protected sites, retained even for this molten-globule-like helical structure). H/D exchange does

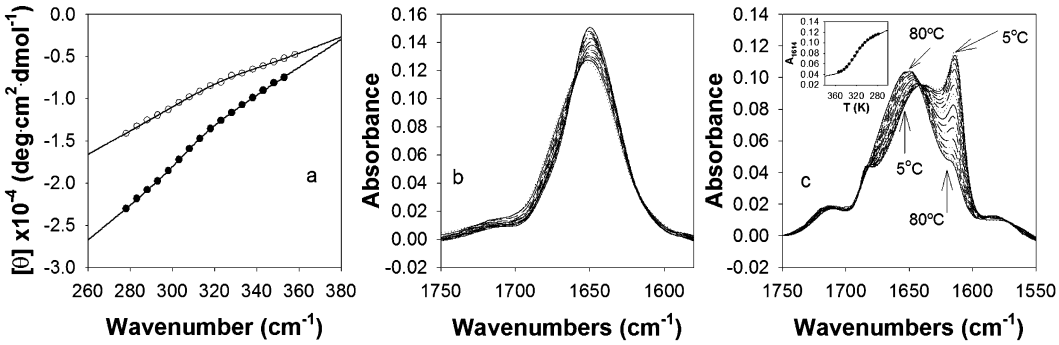


FIGURE 6: (a) Thermal denaturation of Con A in 50% TFE, as monitored by the ellipticity change at 222 nm with ECD (circles) at pH 6.5 (open symbols) and pH 2.1 (filled symbols). No aggregation was observed in this temperature range, and a simple loss of helical CD band shape was seen with an isodichroic point at ~202 nm. (b) Thermal denaturation of Con A in 50% TFE-OD at pH 1.8 as monitored with FTIR. Again no aggregation was observed (by contrast, Con A in just $D_2O$ at pH 1.8 aggregated at high temperature, as indicated by a sharp absorption band at 1620 cm$^{-1}$). (c) Thermal behavior (from 80 to 5 °C) of 10 mg/mL Con A in 50% TFE at pH 3.4, in which the aggregation peak grows with the decrease of temperature. The changes of IR absorbance at 1614 cm$^{-1}$ are plotted as an inset and were fit to a two-state transition expression, resulting in $T_m = 327$ K and $\Delta H = 20 \pm 2$ kcal/mol.

affect the amide I′ of the TFE-induced helical form, which is why its impact is seen on the spectrum for the refolded state, although it has minimal impact on the native, predominantly $\beta$-sheet form or on the high-temperature unfolded form. In a parallel experiment (not shown), Con A in only aqueous (no TFE) solution at pH 1.8 developed an aggregation peak with heating, evidenced by an absorption band at 1620 cm$^{-1}$ sharply increasing in intensity between 40 and 55 °C.

Thermal unfolding of Con A in 50% TFE at a higher pH, 3.4, where the FTIR spectra show evidence of both α-helix and aggregation components, was also monitored with FTIR, as shown in Figure 6c. With an increase of temperature, the aggregation features at both 1614 and 1684 cm$^{-1}$ actually lose intensity, while the central band grows and shifts to higher wavenumber, reaching 1651 cm$^{-1}$ at $T = 80$ °C. Thus, in an unusual course of structure variation, the aggregate becomes destabilized at high temperatures and a partially helical form becomes dominant. (A reviewer has noted that the IR alone could be explained by a sheet-to-coil transition. CD data of the same sample used for IR show that the sample is partially helical at low temperature, and loses some but retains much of its elipticity at 222 nm on heating, converting to a helical shape. The degree of helicity sharply depends on concentration and pH, being highly helical at low concentration and lower pH. While the loss of sheet seen in Figure 6c is a clear sigmoidal shift in equilibrium, the helix change with temperature, as seen in far-UV−CD, is more gradual, nearly linear. Thus, the thermal transition is complex, involving increased disorder as well as sheet to helix conversion.) When temperature decreases, a reversible change is recorded and the spectra are mostly recovered. A near isosbestic point at ~1641 cm$^{-1}$ suggests the process could be approximated as a two-state transition. The intensity change at 1614 cm$^{-1}$ was plotted as an inset in Figure 6c. This change was fit (solid line) by assuming a two-state transition model, resulting in $T_m = 326.6$ K with $\Delta H$ and $\Delta S$ values of 19.8 ± 2.3 kcal/mol and 61 ± 7 cal/mol, respectively, for the transition from this aggregated state, pH 3.4 in 50% TFE.

*Stopped-Flow CD and Fluorescence Experiments*. Stopped-flow CD for Con A unfolding with TFE (1:1) was measured at $T = 25$ °C and pH 2.0 (circles), 4.5 (squares), and 6.7 (triangles), as shown in Figure 7a, by monitoring the ellipticity change at 222 nm, to sense the gain of α-helix content with added TFE. All three were fit to exponential curves, and the derived rate constants are presented in Table 1. While a single-exponential curve can fit the change at pH 4.5, double-exponential behavior gives a better fit for pH 2.0 and 6.7; however, such multiexponential changes do not necessarily demonstrate the involvement of an intermediate. Without TFE, a 1:1 dilution of Con A in $H_2O$ results in no detectable time-dependent ellipticity change as seen in the top trace of Figure 7a. This ellipticity value can be used as a reference for all pH conditions since the ellipticity at 222 nm for Con A in $H_2O$ is independent of pH as shown in

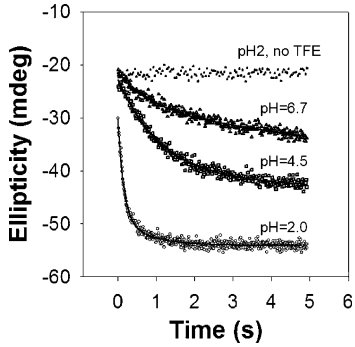


FIGURE 7: (a) Stopped-flow far-UV−CD change recorded at 222 nm for Con A ($C_f = 0.2$ mg/mL) mixing with TFE at pH 6.7 (△), 4.5 (□), and 2.0 (○). The ellipticity of Con A in the absence of TFE (filled dots, no change with time) was also plotted as a comparison. The solid lines are fits to the ellipticity changes. All the spectra are recorded with a data pitch of 2 ms and are averages of 20 shots. Corresponding kinetic blanks were obtained by mixing just $H_2O$ and TFE under the same conditions and were subtracted to obtain the final stopped-flow changes.

Table 1: Parameters of Stopped-Flow CD for Concanavalin A Mixing with TFE[a]

| Con A + TFE | $a_1$ (100%) | $k_1$ (s$^{-1}$) | $a_2$ (100%) | $k_2$ (s$^{-1}$) |
|---|---|---|---|---|
| pH 6.7, 222 nm | 0.23 | 2.17 | 0.77 | 0.34 |
| pH 4.5, 222 nm | 1.0 | 0.82 | | |
| pH 2.0,[b] 222 nm | 0.62 | 6.85 | 0.17 | 1.38 |

[a] Results of fitting kinetic curves to two (or one) exponentials in the form of $Y = Y_0 + c_1 \exp(-k_1 t) + c_2 \exp(-k_2 t)$, where $a_1 = c_1/(c_1 + c_2)$ and $a_2 = c_2/(c_1 + c_2)$. [b] A total of 21% of the change is completed within the mixing dead time.

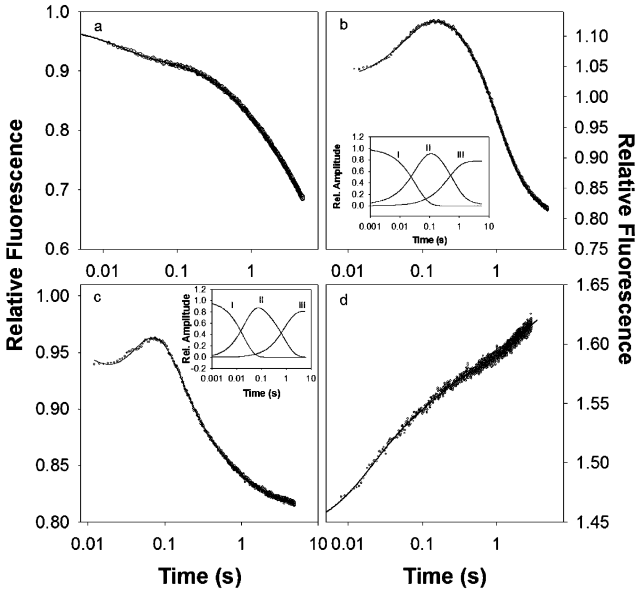


FIGURE 8: Semilog plots of stopped-flow relative fluorescence (RF) changes for denaturing Con A by mixing with TFE (1:1) at pH 6.7 (a), 4.5 (b), and 2.0 (c), for which RF = $(F_{Con+TFE} - F_{H_2O+TFE})/(F_{Con+H_2O} - F_{H_2O})$, where $F_{Con+TFE}$, $F_{H_2O+TFE}$, $F_{Con+H_2O}$, and $F_{H_2O}$ are the kinetic fluorescence amplitudes of Con A mixing with TFE, $H_2O$ mixing with TFE, Con A mixing with $H_2O$, and only $H_2O$, respectively. (d) Stopped-flow fluorescence change of refolding Con A initially in 50% TFE at pH 2 which was then diluted (1:4) with $H_2O$ (pH 2), resulting in a final [TFE] of 10% (v/v). The solid lines are the fits for the fluorescence changes. Insets in (b) and (c) represent the multiple components of the corresponding fluorescence change.

Figure 3 and reported by others (*29*). For pH 6.7 and 4.5, no significant burst-phase CD is observed within the ~11 ms dead time; however, at pH 2, some initial ellipticity loss is observed.

The corresponding stopped-flow fluorescence changes, which monitor the time variation of protein tertiary structure (*38*, *39*), are more complex, as shown in Figure 8, where semilog plots are used to bring out the separate components. When pH is 6.5 (Figure 8a), the fluorescence decay can be fit well with a triple-exponential relationship, and no significant fast change is evident within the mixing dead time (~11 ms, due to apparatus constraint). When pH is 4.5 (Figure 8b) and 2.0 (Figure 8c), a fluorescence intensity increase followed by a slower decay is observed, the main difference between the two pH values being the time needed to reach the maximum signal, ~80 and ~200 ms for pH 2.0 and 4.5, respectively. Again, no significant burst phase (<5−6%) is observed for the fluorescence change at these two pH values, which is consistent with little very fast change for pH 2 as detected by stopped-flow CD at 290 nm (data not shown). The fluorescence change can be fit with a multiexponential curve, two components of which correspond to a fluorescence increase while the rest yield decay. They can be assigned, although somewhat arbitrarily, to three major components as shown in the insets, corresponding to the change of reactant, intermediate, and product, as presented in Table 2. The multiexponential curve assigned to the change of intermediate is reasonable, considering the existence of four Trp residues in each monomer and the complex kinetic variation in fluorescence (Figure 8a−c) observed. Nonetheless, one should recognize that the reliability of the smaller components is naturally questionable (see the Discussion). The major kinetic components in the pH 2.0 and 6.7 fluorescence changes (Table 2) have a parallel in the simpler CD changes (Table 1), but the comparison of the pH 4.5 results is less clear.

A separate experiment indicates that the nativelike CD spectrum can be recovered when the TFE-induced (50%) α-helical state is diluted with $H_2O$ to a solution containing <10% TFE. Results of a refolding experiment for diluting Con A at pH 2 in TFE (50%) with $H_2O$ at the same pH are shown in Figure 8d. For refolding, a fluorescence increase is observed, which can be fit with a triple-exponential curve. Additionally, a big fluorescence change (~45%) occurs within the mixing dead time (~5 ms, due to the use of different syringes for refolding). The corresponding far-UV−CD change at 222 nm does not show any measurable slow change for refolding, but only a very fast secondary structure change (α-helix to β-sheet) which is complete within the mixing dead time (data not shown). A control experiment, mixing Ala-Trp-Ala in $H_2O$ with TFE, shows it to have a neglectable fluorescence change compared with the change observed in the above tests, eliminating the possibility of this being an intrinsic Trp fluorescence change caused by a solvent effect.

*Dynamic Solvent Mixing with FTIR.* Some of the ECD results, measured at low concentration and which are sensitive to long-range order, do not appear to agree with the FTIR data from high-concentration samples which have shorter range order dependence. For example, at neutral pH, concanvalin A in 50% TFE shows stable α-helical ECD over a short time scale, while with higher concentrations precipitation is observed immediately at neutral pH. At pH ≈ 4, FTIR shows aggregation developing more slowly (judged by the ~1616 $cm^{-1}$ band intensity) followed by precipitation, both indicating the formation of β-structure.

To further explore this, a stopped-flow FTIR experiment was carried out by rapidly mixing Con A at pH 3.7 with TFE-OD. The time-resolved FTIR spectra were recorded over the full spectrometric range but are only presented here for the interval from 1600 to 1700 $cm^{-1}$, the amide I′ band region. Although slower in time resolution than the previous fluorescence and CD stop-flow measurements, a fast change within seconds and a slow change after 1 min were recorded, as shown in Figure 9. In the fast change, a β-sheet to α-helix transition was observed, as shown in the difference spectra in Figure 9a by the disappearance of a component at 1634 $cm^{-1}$ and the growth of one at 1652 $cm^{-1}$. Because of the poor S/N of these IR spectra, which are each the result of only a single scan (no averaging), it is impossible to obtain more reliable information directly from these individual IR spectra. However, by factor analysis (FA, or equivalently principle component analysis, PCA (*26*)) of the time-dependent spectra, we can effectively average over the entire band shape, determining its global change, and thereby derive quantitative kinetic information while filtering out undesired interference caused by noise and residual water vapor. FA of a set of related spectra generates a set of component spectra which can be used to reconstruct each input spectrum as a linear combination of the components, weighted by loading factors. The first component spectrum will be approximately the average of the set, and the second will be the main variance from it. The loading of the second

Table 2: Parameters of Stopped-Flow Fluorescence for Concanavalin A Mixing with TFE[a,b]

| Con A + TFE | | $a_1$ (100%) | $k_1$ ($s^{-1}$) | $a_2$ (100%) | $k_2$ ($s^{-1}$) | $a_3$ (100%) | $k_3$ ($s^{-1}$) | $a_4$ (100%) | $k_4$ ($s^{-1}$) |
|---|---|---|---|---|---|---|---|---|---|
| pH 6.7 | | 0.13 | 61.4 | 0.17 | 1.52 | 0.70 | 0.18 | | |
| pH 4.5 | curve I | 1.0 | 28.8 | | | | | | |
| | curve II | −1.0 | 26.61 | 0.91 | 1.73 | 0.09 | 0.22 | | |
| | curve III | −1.0 | 2.24 | | | | | | |
| pH 2.0 | curve I | 1.0 | 53.2 | | | | | | |
| | curve II | −1.0 | 44.3 | 0.15 | 8.7 | 0.80 | 1.26 | 0.05 | 0.48 |
| | curve III | −1.0 | 1.21 | | | | | | |

[a] Results of fitting kinetic curves to multiple exponentials in the form of $Y = Y_0 + c_1 \exp(-k_1 t) + c_2 \exp(-k_2 t) + \ldots + c_n \exp(-k_n t)$, where $a_n = c_n/(c_1 + c_2 + \ldots + c_n)$. [b] A negative sign of amplitude indicates a fluorescence increase instead of decay.

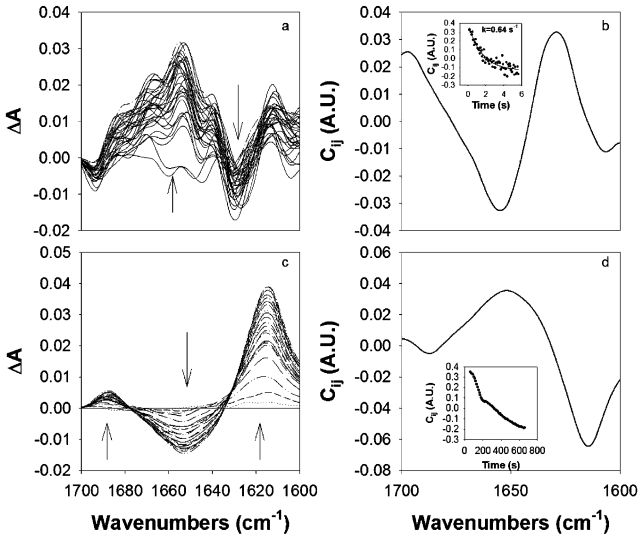


FIGURE 9: (a) Stopped-flow difference amide I′ IR spectra for Con A at pH 3.7 as denatured by addition of 50% TFE-OD. The spectra were obtained from the time-dependent absorbance spectra according to $S_n - S_1$, where $S_n$ is the *n*th scan and $S_1$ is the first IR spectrum scan collected ∼100 ms after mixing when cell fluctuation is complete. (b) Second component spectrum of the whole amide I′ band (1600−1700 $cm^{-1}$) resulting from factor analysis of the change in (a). The corresponding change in its loading is plotted as an inset, and the change was fit with a single-exponential curve. Only half of the spectra ($n \approx 60$) in the first ∼5 s out of a total of ∼200 for ∼10 s were used for the analysis due to a limitation on the matrix size. (c) Difference spectra of the slow changes of Con A at pH 3.7 with added 50% TFE-OD, obtained starting from 1 min after the rapid mixing in (a). Each spectrum was averaged for 5 s, and data shown are for every 10 s. (d) Second component spectrum of the whole-band (1600−1700 $cm^{-1}$) factor analysis results for the change in (c). The corresponding loading is plotted as an inset, the change could be fit with a sigmoidal change for $t < 220$ s, and a single-exponential curve fits the longer time change after that. Arrows in the figures show the direction of change.

component plotted as a function of the perturbation, which is here time, then reflects the major changes in the spectral band shapes being analyzed. The second subspectrum (Figure 9b) obtained by factor analysis of the fast change results has a shape consistent with a 1630 → 1654 $cm^{-1}$ frequency shift, confirming the $\beta \rightarrow \alpha$ transition. The corresponding time-dependent loading values are plotted as an inset in Figure 9b, and can be fit with a single-exponential curve. The result of fitting the variations in the loading of the second component spectrum obtained by factor analysis of the entire amide I′ band for just the fast kinetic changes at three pH values are in Table 3.

Figure 9c shows the difference spectra corresponding to the slow change, which was obtained starting 1 min after the rapid mixing. Here due to slower data acquisition, the individual spectra (obtained over 5 s, averaging ∼40 scans) are more reliable. A decrease of the amide I′ intensity at 1651 $cm^{-1}$ (negative band) was obtained, accompanied by growth of aggregation, as indicated by the (positive) peaks at 1615 and 1685 $cm^{-1}$. The second subspectrum of the factor analysis for just this slow change (Figure 9d) confirms the α-helix to aggregate (extended $\beta$-sheet structure) transition. The corresponding time dependence of the loading is plotted as an inset in Figure 9d, but this complex change has to be analyzed in parts, suggesting a multistage aggregation mechanism is involved. The early stage can be described by a sigmoidal change ($t_m \approx 142$ s), while the later stage can be fit with a single-exponential change ($k = 0.0025$ $s^{-1}$). The point used for separating the analyses of these two stages was ∼220 s, which is somewhat arbitrary due to the concurrent reactions in this time region. This behavior is consistent with an induction period in which an intermediate population grows to a level to sustain the aggregation reaction. Such behaviors are seen in amyloid-forming proteins under certain conditions (*6*, *21*). Fast mixings at other pHs were also tested with FTIR. At pH 4.1, a fast $\beta \rightarrow \alpha$ transformation was observed, but the aggregation peak grew in much faster than at pH 3.7, and precipitation eventually caused loss of signal. At pH 2, only the fast $\beta \rightarrow \alpha$ transition was obtained, but it was fit best with a double exponential, and no slow intermediate equilibrium was evident.

Table 3: Parameters of Stopped-Flow FTIR for Concanavalin A Mixing with TFE[a]

| Con A + TFE | $a_1$ (100%) | $k_1$ ($s^{-1}$) | $a_2$ (100%) | $k_2$ ($s^{-1}$) |
|---|---|---|---|---|
| pH 4.1 | 1.0 | 0.51 | | |
| pH 3.7 | 1.0 | 0.64 | | |
| pH 2.0 | 0.41 | 3.08 | 0.59 | 0.53 |

[a] Results of the fit (to the equation in Table 1) of the variation in the loading of the second component spectrum obtained by factor analysis of the entire amide I′ band (see the text) for just the fast kinetic changes (e.g., Figure 9b, measured to 10 s) at three pH values.

## DISCUSSION

*Properties of TFE-Induced α-Helical Con A.* Although the native-state Con A secondary structure is predominantly $\beta$-sheet with no α-helix, the sequence must have some helical propensity, since with the addition of 50% TFE a mainly α-helical structure is obtained, the helical content reaching ∼57% at pH 2. For comparison, $\beta$-lactoglobulin, which has a quite different $\beta$-sheet native fold and stability and whose

sequence is predicted to have some helical propensity (*40*), also has a high helical content with TFE (*4*). These two examples suggest that conversion to helical dominance in TFE should not be unexpected for some $\beta$-sheet proteins.

The far-UV−CD results indicate that the secondary structure of Con A in aqueous solution is independent of the solution pH, but the near-UV−CD and fluorescence suggest that the Trp residues can change, by either protonation or a partial opening (solvation) of the tertiary structure. By contrast, in 50% TFE, Con A is more α-helical at pH 2 than at neutral pH, and the low-pH helical form is more stable (in terms of resisting aggregation) than at intermediate pH, which suggests that the protonated polypeptide chain has a higher tendency to form an α-helix in this specific case. As determined by FTIR, the TFE-induced α-helical form of Con A is stable at pH 2, while at pH 3−4, aggregation effects are seen, and precipitation appears when pH > 4. These results indicate that pH has a big effect on the structure and stability of the TFE-denatured state of Con A, in contrast to the very small effect on the native, aqueous state. Clearly, it is not just the presence of the charged groups but also their position in the final three-dimensional structure of the protein that affects its stability (*41*). Lack of charge (e.g., protonating acidic groups) would be expected to lead to protein aggregation, while adding charge (e.g., to basic groups) should enhance solubility and coil formation. That in TFE−$H_2O$ one can get more stable helix formation at low pH suggests that indiscriminate protonation is not the operative mechanism. However, aggregation at pH ≈ 4 implies the protonation is important once the protein tertiary structure is relaxed via TFE addition.

Protein concentration is found to be another factor for the conformation and stability of the TFE-denatured state of Con A. At low protein concentration, as is typical for ECD measurement, only an α-helical-type spectrum is observed initially, precipitation being observed only after several hours at neutral pH with stirring. However, at high concentration, as needed for FTIR, obvious spectral characteristics of intermolecular $\beta$-sheet structure (aggregation) are obtained in the pH range from 3 to 4, and a precipitate is obtained for pH > 4, indicating that high protein concentration accelerates aggregation as would be expected for a conformational change based on protein−protein interaction. The low-frequency high-intensity IR band at ∼1615 $cm^{-1}$ is indicative of formation of extended, relatively flat antiparallel $\beta$-sheets and has no known spectral equivalent for monomeric intramolecular sheet formation (*42*). ConA has one of the most distinctive $\beta$-sheet amide I′ IR bands known, yet from Figure 4, it is clear that its intramolecular sheets have transitions clearly distinguishable from those of an aggregate.

Normally, high temperature will induce aggregate formation, due to exposure of hydrophobic residues; however. in this study, the low-pH TFE-induced α-helical form of Con A has a gradual, noncooperative unfolding (presumably to the coil form) that is not complete by 85 °C. CD indicates residual α-helix at high temperature, and IR shows no aggregation. At pH 3.4, as monitored by FTIR, a surprising reverse transition, aggregation to mixed α-helix and coil, occurs with an increase of temperature and confirms that high temperature can destabilize the aggregate form, breaking up presumably hydrophobically driven interactions dominant at intermediate pH due to loss of tertiary structure. Analysis of this complex structural change fits a simple thermal equilibrium resulting in $\Delta H$ and $\Delta S$ both being positive for a change from the aggregate conformation, suggesting that the final form maintains a higher entropy level with fewer hydrogen bonds than the aggregate, which certainly would be the case for a coil form. However, monomeric conformations with much helix would also have positive $\Delta S$ for this transition, due to the loss of aggregate, extended $\beta$-sheet structures (locally ordered as evidenced by the IR band shape (*42*)).

Although Con A in TFE at low pH has a highly helical conformation, it has no helical segments in its native state, which is very high in $\beta$-sheet content as would be predicted on the basis of its amino acid sequence (*40*). This could also be viewed as being consistent with the observed aggregation of Con A in TFE at neutral pH (FTIR having a strong peak at ∼1616 $cm^{-1}$). However, instead of forming a nativelike intramolecular $\beta$-sheet conformation, with loss of tertiary structure, the intermolecular $\beta$-sheet becomes dominant, as is clear from the shift of the IR bands. Lack of intramolecular $\beta$-structure formation in TFE suggests that fewer portions of the polypeptide tend to form the nativelike $\beta$-sheet in the $H_2O$−TFE environment (as opposed to many strands in the native structure), while the amount of exposed hydrophobic surface area increased, presumably after formation of the helical intermediate, driving the aggregation. In such a case, an energetically competitive possibility for forming $\beta$-sheets is that such segments might "meet" the same portion on another chain, resulting in intermolecular $\beta$-structure, a situation which would be favored at higher protein concentration. This sort of process may be important in amyloid-forming proteins and peptides as well which often aggregate via a helix to sheet transformation.

At very low pH intermolecular interaction becomes disfavored, due to protonation, as evidenced by stabilization of the monomer (*43*). Such a change would also shift the balance from intermolecular $\beta$-sheet H-bond formation to intramolecular helical segment formation in a globular protein. This eliminates the potential aggregate-stabilizing effects of negatively charged (acidic) residues, resulting in electrostatic repulsion between residual positively charged chains. Since the significant change occurs at pH 3−4, Asp and/or Glu (which become neutralized on being protonated when pH < 4.0) could possibly be important residues in that portion of the sequence that changes conformation on an increase of pH. On the basis of the results above, the α-helical dominant form of denatured Con A in TFE appears to be a stable intermediate on this specific unfolding pathway that leads to aggregation in TFE.

*Unfolding Mechanism.* In the stopped-flow fluorescence tests, no significant burst phase is observed at the three pH values studied, suggesting the lack of very fast processes in this unfolding. When Con A is studied under dimer-forming conditions (pH 2.0 and 4.5), after being mixed with TFE, a fluorescence intermediate with increased intensity is seen growing in at 100−200 ms, followed by a slower decay. The fit to this kinetic change can be formulated to follow such a three-state process, in which the measured signal represents the decaying fluorescence of an initial state, an intermediate state growing and decaying, and a final state developing after an induction period. Obviously the fit of the fluorescence to so many exponential components has a

degree of arbitrariness, particularly for kinetic components of small amplitude or those of oppositely signed amplitudes with similar *k* values. These are the best fits we obtained to relatively high S/N data and yield intermediates that do correspond to a logical model.

The fluorescence increase of the intermediate could involve partial burial of some Trp residue which is exposed to solvent in the native state while assuming the rest of the Trp residues remained mostly intact, suggesting that the hydrophobic core of the dimer may still exist. This assumption is partially based on the fact that burial of the Trp side chain in an apolar environment within the native state or in a compact folding intermediate would result in enhancement of fluorescence yield (*44*). The fluorescence decay for the intermediate would then be due to the partial exposure of the remaining Trp residues to the solvent at different rates, resulting from the formation of local non-native secondary structure (α-helix). At the same time the dimer form could dissociate due to destabilization of the *β*-structure holding the subunits together.

The process for TFE solvation of the dimer, $\mathbf{N}_2$, can be described as

$$\mathbf{N}_2 \xrightarrow{\text{TFE}} \mathbf{I} \xrightarrow{\text{TFE}} \mathbf{D^*}\ (\alpha\text{-helical})$$

where **I** is a relatively stable unfolding intermediate with a mostly intact hydrophobic core having more or less α-helical structure dependent on pH, and **D*** is a denatured form having partial α-helical structure but no stable tertiary structure.

In the refolding experiment in which TFE-denatured Con A at pH 2 was diluted with $H_2O$ at the same pH, all the CD change was completed during the mixing dead time (∼5 ms); however, a relatively large fluorescence increase was observable after 5 ms. This shows that the loss of non-native (α-helical) secondary structure is very fast upon solvent perturbation where there is little stable protein tertiary structure, but that tertiary structure recovery is slower.

By contrast to the unfolding experiments at the above two reduced pH values, when pH is 6.7, under which conditions native Con A is a tetramer, a simpler fluorescence decay is observed for the TFE-induced protein unfolding after the mixing dead time, indicating the lack of the long-lived intermediate discussed above. The unfolding process for the tetramer, $\mathbf{N}_4$, could thus be described as

$$\mathbf{N}_4 \xrightarrow{\text{TFE}} \mathbf{D}\ (\alpha\text{-helical})$$

where **D** is also a denatured form having partial α-helical structure, analogous to the **D*** state above but differing in terms of α-helix content (Figure 3a). However, an alternative mechanism cannot be excluded, that involving dissociation of tetramer to monomer within the mixing dead time, but this would require assuming that the monomer has a fluorescence intensity similar to that of the tetramer.

In dimer proteins, if the relative contribution of the intersubunit interactions is weaker than that of the intrasubunit ones, then unfolding may be accompanied by the formation of a stable monomer intermediate, which would follow the process $\mathbf{N}_2 \leftrightarrow 2\mathbf{I} \leftrightarrow 2\mathbf{U}$ and show biphasic denaturation profiles. When intersubunit interactions contribute significantly to the overall stability of the protein, the unfolding may appear to be a simple two-state process, $\mathbf{N}_2 \leftrightarrow 2\mathbf{U}$ (*41*). Chatterjee and Mandal (*45*) reported the existence of Con A monomer at pH 7 after chemical denaturation ($\mathbf{N}_4 \leftrightarrow 4\mathbf{N} \leftrightarrow 4\mathbf{U}$) with low concentration of denaturant (e.g., 2.7 M urea). However, no strong evidence was provided to support the proposal that the monomer intermediate still had the same native conformation as in the tetramer. By contrast, Mitra et al. (*41*) claimed no intermediate on the denaturation of Con A at pH 5 by GuHCl ($\mathbf{N}_2 \rightarrow 2\mathbf{U}$). These results indicate that the intersubunit interaction in dimer form is stronger than that in the tetramer form, which might explain the observation of dissociation of the dimer form in our study and suggest the possibility of tetramer dissociation occurring within the mixing dead time.

In contrast to our stopped-flow CD data, which monitored the secondary structure change only at a single wavelength (222 nm) and thus focused on the α-helix change (*46*, *47*), our stopped-flow FTIR measured the whole amide I band change but with less time resolution (∼50 ms in this case). In addition, FTIR provides a complementary method for stopped-flow CD and fluorescence since it can extend conformational selectivity by monitoring change with high sensitivity to *β*-sheet structure at the cost of demanding a higher protein concentration. Previous stopped-flow FTIR experiments on other proteins have focused on the intensity of single bands (*48*, *49*), and some band shape change measurements were presented with a continuous-flow IR method (*50*). In our study, simultaneous disappearance of *β*-sheet and growth of α-helix were monitored in stopped-flow FTIR, through whole-band analysis, which gives a clearer picture of the structural change than CD.

The stopped-flow FTIR results agree with the stopped-flow CD results for Con A mixing with TFE, both showing a single-exponential change at pH ≈ 4 and a double-exponential change at pH 2. Both sense secondary structure, CD predominantly in terms of α-helix change, but for FTIR, the entire integrated structural shift (*β* → α) is monitored in terms of the loading (contribution) of the second subspectrum. Both also see the same kinetic processes, but with different selectivities. Although the rate constants are quite comparable, they are not the same, which may be due to different methods used (direct, single-frequency intensity measured for CD but whole-band factor analysis for FTIR) and the different concentrations involved. The same unfolding mechanism appears to be detected by both methods, and thus, the form (mechanism) of this process can be viewed as qualitatively independent of protein concentration. We also monitored the disappearance of *β*-sheet and formation of α-helix separately by looking at independent factor analyses of the frequency ranges of 1600−1642 and 1642−1700 $cm^{-1}$, respectively. These results suggest that the disappearance rate of *β*-sheet is faster than the formation of α-helix although the difference was not significant given our experimental uncertainties. This ability of FTIR to look at change in two secondary structure components separately is unique as compared with stopped-flow CD and fluorescence.

The slow change observed in the stopped-flow FTIR after some induction time (∼1 min at pH 3.7) represents a transition from α-helix to an aggregated state. Factor analysis suggests it has two stages, indicating the existence of an intermediate. The first stage, which fits a sigmoidal change, could be described as a multimolecular (two or more)

complex transition from α-helical to intermolecular β-sheet conformation. The second stage, which fits a single-exponential decay, is hard to interpret. Here we tentatively assume an aggregate state is formed by means of a packing rearrangement within this multimolecule cluster, acting as a first-order process; however, further evidence is needed to support such a mechanism. These observations suggest that some region of the sequence forms intermolecular β-structure first, and then that this complex nucleates aggregation of other parts. Such a process may be of relevance to the aggregates formed by many different proteins in amyloid-type processes.

*Mechanism of TFE-Induced Denaturation*. TFE is a slightly stronger proton donor than water but a much weaker proton acceptor (*51*). The dielectric constant of TFE at room temperature is 26, which is significantly smaller than that of water (∼80). However, it is unclear if this low dielectric constant could be responsible for the formation of the α-helical form (*20*, *52*). Theoretical computational results using a two-dimensional lattice model suggest that TFE mainly weakens nonlocal hydrophobic contacts and slightly enhances local helical interactions (*15*). Equilibrium hydrogen isotope partition measurements by Kentsis et al. (*3*) confirmed that the intramolecular hydrogen bonds are not strengthened by TFE; instead they proposed that the helical enhancement by monohydric alcohols is caused by the decrease in the extent of backbone solvation in the unfolded state rather than by the explicit stabilization of hydrogen bonds.

Main and Jackson reported that TFE at low concentration acts mainly as an osmolyte, disrupting the water structure surrounding the protein (*5*). They found that TFE (10%) does not significantly change the folding pathway of FKBP12, so that this effect, rather than being caused by the stabilization of a single element of structure, to them appears to be global in nature, affecting all regions of the protein structure equally. Shiraki et al. (*4*) proposed that the helical propensity of the TFE state is determined by local interaction based on the amino acid sequence. Thomas et al. (*15*) also argued that the effects are sequence dependent because they found that different native structures respond differently to alcohol. However, the opposite conclusion was made by Mantsch et al. (*20*) that the helix formation appeared to be primarily due to properties of the solvent and not of the polypeptide chain.

In our experiments, addition of TFE disrupts the native structure of Con A and induces the formation of an α-helical form. Limited addition of TFE (∼10%) will first change its CD from a band shape atypical to one typical of β-sheet, suggesting TFE affects the nonlocal intramolecular hydrophobic interactions that might cause structural restrictions for aromatic side chains, which consequently would yield CD components that interfere with secondary-structure-sensitive amide bands in the near-UV. More addition of TFE will then destroy the native structure and induce formation of an α-helical conformation, which is sensitive to the solution conditions (e.g., pH and protein concentration). The tendency of this state to form an intermolecular β-sheet conformation suggests a loss of compactness, resulting in exposure of hydrophobic segments, and would be consistent with the helicity in TFE being sequence dependent (*4*). The formation of the monomeric (intermediate) α-helical form would then be due to the disruption of long-range hydrophobic interactions, which will in turn allow local helical interactions to provide a transient means of decreasing backbone solvation before aggregation, requiring interprotein bonding and eventually providing a deeper energy minimum. The stopped-flow dilution of TFE-induced Con A at pH 2 also suggests that the TFE-denatured state may have an open-helical structure in which the interactions between helical segments are weak as reported in other TFE−protein systems (*4*).

## CONCLUSION

The conformational change of Con A as affected by the addition of TFE is studied systematically in this paper. This system (the dimer form of Con A with TFE) has proven to be a good model due to its relatively slow kinetic changes, which can be monitored by several time-resolved methods (CD, fluorescence, and IR). Complex changes ($\beta \rightarrow \alpha \rightarrow \beta$) were observed, and several intermediates were detected on the unfolding pathway, including the $H^+$-stabilized α-helical form. In particular, time-resolved FTIR spectroscopy can utilize the advantage of measuring a complete spectrum for each time point of measurement without much loss of time resolution. In this way, the disappearance of β-sheet and growth of α-helix are monitored directly and simultaneously in FTIR, which is a unique characteristic in contrast to other techniques such as CD and fluorescence. Stopped-flow FTIR has a great potential to complement the established kinetic techniques in describing structural events and should have a wide range of applications.

## ACKNOWLEDGMENT

We thank Dr. Xiuqi Zhang for aid in confirming some of the experimental results and Prof. Anjum Ansari for granting us access to her fluorimeter.

## REFERENCES

1. Vannuland, N. A. J., Chiti, F., Taddei, N., Raugei, G., Ramponi, G., and Dobson, C. M. (1998) Slow Folding of Muscle Acylphosphatase in the Absence of Intermediates, *J. Mol. Biol. 283*, 883−891.
2. Buck, M., Radford, S. E., and Dobson, C. M. (1993) A Partially Folded State of Hen Egg White Lysozyme in Trifluoroethanol: Structural Characterization and Implication for Protein Folding, *Biochemistry 32*, 669−678.
3. Kentsis, A., and Sosnick, T. R. (1998) Trifluoroethanol promotes Helix Formation by Destabilizing Backbone Exposure: Desolvation Rather Than Native Hydrogen Bonding Defines the Kinetics Pathway of Dimeric Coiled Coil Folding, *Biochemistry 37*, 14613−14622.
4. Shiraki, K., Nishikawa, K., and Goto, Y. (1995) Trifluoroethanol-induced Stabilization of the Alpha-helical Structure of Beta-Lactoglobulin: Implication for Non-hierachical Protein Folding, *J. Mol. Biol. 245*, 180−194.
5. Main, E. R. G., and Jackson, S. E. (1999) Does Trifluoroethanol Affect Folding Pathways and Can it Be Used as Probe of Structure in Transition States? *Nat. Struct. Biol. 6*, 831−835.
6. Srisailam, S., Kumar, T. K., Rajalingam, D., Kathir, K. M., Sheu, H. S., Jan, F. J., Chao, P., and Yu, C. (2003) Amyloid-like Fibril Formation in an All -Barrel Protein. Partially Structured Intermediate State(s) is A Precursor for Fibril Formation, *J. Biol. Chem. 278*, 17701−17709.
7. Naseem, F., and Khan, R. H. (2004) Fluoroalcohol-induced Stabilization of the −Helical Intermediates of Lentil Lectin: Implication for Non-Hierarchical Lectin Folding, *Arch. Biochem. Biophys. 431*, 215−223.

8. Pallares, I., Vendrell, J., Aviles, F. X., and Ventura, S. (2004) Amyloid Fibril Formation by Partially Structured Intermediate State of Alpha-Chymotrymotrypsin, *J. Mol. Biol. 342*, 321−331.
9. Misumi, Y., Terui, N., and Yamamoto, Y. (2002) Structural Characterization of Non-native States of Sperm Whale Myoglobin in Aqueous Ethanol or 2,2,2-Trifluoroethanol Media, *Biochim. Biophys. Acta 160*, 75−84.
10. Taddei, N., Chiti, F., Fiaschi, T., Bucciantini, M., Capanni, C., Stefani, M., Serrano, L., Dobson, C. M., and Ramponi, G. (2000) Stabilization of −Helices by Site-directed Mutagenesis Reveals the Importance of Secondary Structure in the Transition State for Acylphosphatase Folding, *J. Mol. Biol. 300*, 633−647.
11. Luo, P., and Baldwin, R. L. (1997) Mechanism of Helix Induction by Trifluoroethanol: A Framework for Extrapolating the Helix-Forming Properties of Peptides from Trifluoroethanol/Water Mixtures Back to Water, *Biochemistry 36*, 8413−8421.
12. Luo, Y., and Baldwin, R. L. (1998) Trifluoroethanol Stabilize the pH4 Folding Intermediate of Sperm Whale Apomyoglobin, *J. Mol. Biol. 279*, 49−57.
13. Segawa, S. I., Fukuno, T., Fujiwara, K., and Noda, Y. (1991) Local Structures in Unfolded Lysozyme and Correlation with Secondary Structures in the Native Conformation: Helix-forming or Breaking Propensity of Peptide Segments, *Biopolymers 31*, 497−509.
14. Dyson, H. J., and Wright, P. E. (1993) Peptide Conformation and Protein Folding, *Curr. Opin. Struct. Biol. 3*, 60−65.
15. Thomas, P. D., and Dill, K. A. (1993) Local and Nonlocal Interactions in Globular Proteins and Mechanisms of Alcohol Denaturation, *Protein Sci. 2*, 2050−2065.
16. Lis, H., and Sharon, N. (1998) Lectins: Carbohydrate-specific Proteins That Mediate Cellular Recognition, *Chem. Rev. 98*, 637−674.
17. Parkin, S., Rupp, B., and Hope, H. (1996) Atomic Resolution Structure of Concanavalin A at 120 K, *Acta Crystallogr. D52*, 1161−1168.
18. Srinivas, V. R., Reddy, G. B., Ahmand, N., Swaminathan, C. P., Mitra, N., and Surolia, A. (2001) Legume Lectin Family, the 'Natural Mutants of the Quaternary State' Provide Insight into the Relationship Between Protein Stability and Oligomerization, *Biochim. Biophys. Acta 1527*, 102−111.
19. Pflumm, M. N., and Beychok, S. (1974) Alkali and Urea Induced Conformation Changes in Concanavalin A, *Biochemistry 13*, 4982−4987.
20. Jackson, M., and Mantsch, H. H. (1992) Halogenated Alcohols as Solvent for Proteins: FTIR Spectroscopic Studies, *Biochim. Biophys. Acta 1118*, 139−143.
21. Khurana, R., Gilleppie, J. R., Talapatra, A., Minert, L. J., Jonesiu-Zanetti, C., Millett, I., and Fink, A. L. (2001) Partially Folded Intermediates as Critical Precursors of Light Chain Amyloid Fibrils and Amorphous Aggregates, *Biochemistry 40*, 3525−3535.
22. Booth, D. R., Sunde, M., Belloti, V., Robinson, C. V., and Hutchinson, W. L. (1997) Instability, Unfolding and Aggregation of Human Lysozyme Variants Underlying Amyloid Fibrillogenesis, *Nature 385*, 787−793.
23. Kelly, J. W. (1998) The Environmental Dependency of Protein Folding Best Explains Prion and Amyloid Disease, *Proc. Natl. Acad. Sci. U.S.A. 95*, 930−932.
24. Fink, A. L. (1998) Protein Aggregation: Folding Aggregates, Inclusion Bodies and Amyloid, *Folding Des. 3*, 9−23.
25. Dobson, C. M., Evans, P. A., and Radford, S. E. (1994) Understanding How Proteins Fold- The Lysozyme Story So Far, *Trends Biochem. Sci. 19*, 31−37.
26. Malinowski, E. R. (1991) *Factor Analysis in Chemistry*, 2nd ed., Wiley, New York.
27. Baumruk, V., Pancoska, P., and Keiderling, T. A. (1996) Predictions of Secondary Structure Using Statistical Analyses of Electronic and Vibrational Circular Dichroism and Fourier Transform Infrared Spectra of Proteins in $H_2O$, *J. Mol. Biol. 259*, 774−791.
28. Wi, S., Pancoska, P., and Keiderling, T. A. (1998) Predictions of Protein Secondary Structures Using Factor Analysis on Fourier Transform Infrared Spectra−Effect of Fourier Self-deconvolution of the Amide I and Amide II Bands, *Biospectroscopy 4*, 93−106.
29. Fink, A. L., Calciao, L. J., Goto, Y., Kurotsu, T., and Palleros, D. (1994) Classification of Acid Denaturation of Proteins: Intermediates and Unfolded States, *Biochemistry 33*, 12504−12511.
30. Xu, Q. (2004) Ph.D. Thesis, Department of Chemistry, University of Illinois at Chicago, Chicago, IL.
31. Sreerama, N., Venyaminov, S. Y., and Woody, R. W. (1999) Estimation of the Number of α-Helical and *β*-Sheet Strand Segments in Proteins Using Circular Dichroism Spectroscopy, *Protein Sci. 8*, 370−380.
32. Pinheiro, T. J. T., Elove, G. A., Watts, A., and Roder, H. (1997) Structural and Kinetic Description of Cytochrome *c* Unfolding Induced by the Interaction with Lipid Vesicles, *Biochemistry 36*, 13122−13132.
33. Burnstein, E. A., Vedenkina, N. S., and Ivkova, M. N. (1973) Fluorescence and the Location of Tryptophan Residues in Protein Molecules, *Photochem. Photobiol. 18*, 263−279.
34. Kuwajima, K. (1996) The Molten Globule State of Alpha-Lactalbumin, *FASEB J. 10*, 102−109.
35. Gupta, P., Khan, R. H., and Saleemuddin, M. (2003) Trifluoroethanol-induced "Molten Globule" State in Stem Bromelain, *Arch. Biochem. Biophys. 413*, 199−206.
36. Jackson, M., and Mantsch, H. H. (1995) The Use and Misuse of FTIR Spectroscopy in the Determination of Protein Structure, *Crit. Rev. Biochem. Mol. Biol. 30*, 95−120.
37. Ismail, A. A., Mantsch, H. H., and Wong, P. T. (1992) Aggregation of Chymotrypsinogen: Portrait by Infrared Spectroscopy, *Biochim. Biophys. Acta 1121*, 183−188.
38. Shastry, M. C. R., Sauder, J. M., and Roder, H. (1998) Kinetic and Structural Analysis of Submillisecond Folding Events in Cytochrome c, *Acc. Chem. Res. 31*, 717−725.
39. Shastry, M. C. R., and Roder, H. (1998) Evidence for Barrier-Limited Protein Folding Kinetics on the Microsecond Time Scale, *Nat. Struct. Biol. 5*, 385−392.
40. Nishikawa, K., and Noguchi, T. (1991) Predicting Protein Secondary Structure Based on Amino Acid Sequence, *Methods Enzymol. 202*, 31−44.
41. Mitra, N., Srinivas, V. R., Ramya, T. N. C., Ahmad, N., Reddy, B. G., and Surolia, A. (2002) Conformational Stability of Legume Lectins Reflect Their Different Modes of Quaternary Association: Solvent Denaturation Studies on Concanavalin A and Winged Bean Acidic Agglutinin, *Biochemistry 41*, 9256−9263.
42. Kubelka, J., and Keiderling, T. A. (2001) Differentiation of Beta-Sheet-forming Structures: Ab Initio-Based Simulations of IR Absorption and Vibrational CD for Model Peptide and Protein Beta-Sheets, *J. Am. Chem. Soc. 123*, 12048−12058.
43. Xu, Q., and Keiderling, T. A. (2004) Optical Spectroscopic Differentiation of Various Equilibrium Denatured States of Horse Cytochrome c, *Biopolymers 73*, 716−726.
44. Lakowicz, J. R. (1991) *Topics in fluorescence spectroscopy: volume 2−principles*, Plenum Press, New York.
45. Chatterjee, A., and Mandal, D. K. (2003) Denaturant-induced Equilibrium Unfolding of Concanavalin A is Expressed by a Three-state Mechanism and Provides an Estimate of Its Protein Stability, *Biochim. Biophys. Acta 1648*, 174−183.
46. Kuwajima, K. (1996) Stopped flow Circular Dichroism, in *Circular Dichroism and the Conformational Analysis of Biomolecules* (Fasman, G. D., Ed.) pp 159−182, Plenum, New York.
47. Kuwajima, K., Yamaya, H., Miwa, S., Sugai, S., and Nagamura, T. (1987) Rapid Formation of Secondary Structure Framework in Protein Folding Studied by Stopped-flow Circular Dichroism, *FEBS Lett. 221*, 115−118.
48. White, A. J., Drabble, K., and Wharton, C. W. (1995) A Stopped-Flow Apparatus for IR Spectroscopy of Aqueous Solutions, *Biochem. J. 306*, 843−849.
49. Reinstadler, D., Fabian, H., Backmann, J., and Naumann, D. (1996) Refolding of Thermally and Urea-Denatured Ribonuclease A Monitored by Time-resolved FTIR Spectroscopy, *Biochemistry 35*, 15822−15830.
50. Kauffmann, E., Darnton, N., Austin, R. H., Batt, C., and Gerwert, K. (2001) Lifetimes of Intermediates in the Beta-Sheet to Alpha-Helix Transition of Beta-Lactoglobulin by Using a Diffusional IR mixer, *Proc. Natl. Acad. Sci. U.S.A. 98*, 6646−6649.
51. Llinas, M., and Klein, M. P. (1975) Charge Relay at the Peptide Bond: A Proton Magnetic Resonance Study of Solvent Effects on the Amide Electron Density Distribution, *J. Am. Chem. Soc. 97*, 4731−4737.
52. Nelaon, J. W., and Kallenbach, N. R. (1986) Stabilization of the Ribonuclease S-Peptide Alpha-Helix in Trifluoroethanol, *Proteins: Struct., Funct., Genet. 1*, 211−217.


BI050003U